Circulation and long-term fate of functionalized, biocompatible single-walled carbon nanotubes in mice probed by Raman spectroscopy

Zhuang Liu*, Corrine Davis†, Weibo Cai‡, Lina He‡, Xiaoyuan Chen‡, and Hongjie Dai*§

*Department of Chemistry, Stanford University, Stanford, CA 94305; †Department of Comparative Medicine, Stanford University School of Medicine, Stanford, CA 94305; and ‡The Molecular Imaging Program at Stanford (MIPS), Department of Radiology and Bio-X Program, Stanford University School of Medicine, Stanford, CA 94305

Edited by Charles M. Lieber, Harvard University, Cambridge, MA, and approved December 17, 2007 (received for review August 14, 2007)

Carbon nanotubes are promising new materials for molecular delivery in biological systems. The long-term fate of nanotubes intravenously injected into animals *in vivo* is currently unknown, an issue critical to potential clinical applications of these materials. Here, using the intrinsic Raman spectroscopic signatures of single-walled carbon nanotubes (SWNTs), we measured the blood circulation of intravenously injected SWNTs and detect SWNTs in various organs and tissues of mice *ex vivo* over a period of three months. Functionalization of SWNTs by branched polyethyleneglycol (PEG) chains was developed, enabling thus far the longest SWNT blood circulation up to 1 day, relatively low uptake in the reticuloendothelial system (RES), and near-complete clearance from the main organs in ≈2 months. Raman spectroscopy detected SWNT in the intestine, feces, kidney, and bladder of mice, suggesting excretion and clearance of SWNTs from mice via the biliary and renal pathways. No toxic side effect of SWNTs to mice was observed in necropsy, histology, and blood chemistry measurements. These findings pave the way to future biomedical applications of carbon nanotubes.

biodistribution | blood circulation | nanoparticles | excretion | toxicity

The utilization of novel nanomaterials for biological and biomedical applications has been an active and exciting direction of research in recent years (1–3). A wide range of nanomaterials, such as nanoparticles (4–7), nanorods (8), nanowires (9), and nanotubes (10–12) have been investigated for their potential clinical applications in diagnosis and therapeutic treatment of diseases. The interesting structural, chemical, electrical, and optical properties of carbon nanotubes (13, 14), when used in biological and medical settings, may bring new opportunities to biological detection, imaging, and therapy with high performance and efficacy. Carbon nanotube-based intercellular molecular delivery vehicles have been developed for intracellular gene (15–17) and drug delivery *in vitro* (18, 19). Recently, research began to investigate the behavior of carbon nanotubes in animal bodies *in vivo* (20, 21), including the finding of lack of toxicity of well PEGylated single-walled carbon nanotubes (SWNTs) in mice in a pilot study (M. L. Schipper, N. Nakayama-Ratchford, C.D., N. W. S. Kam, P. Chu, Z.L., X. Sun, L. C. Cork, H.D., and S. S. Gambhir, unpublished data).

The biodistribution of intravenously injected carbon nanotubes in mice has been studied by using radiolabeling and isotope ratio mass spectroscopy methods (20, 22). Promising result of efficient targeted tumor accumulation *in vivo* has been obtained by conjugating a ligand peptide to nanotubes to recognize receptors on the surface of tumor cells (20), suggesting high potential of nanotube-based drug delivery vehicles for cancer therapy. However, an important unaddressed question for carbon nanotubes and various nanomaterials in general in biomedical applications is their long term fate *in vivo*. It is known that most nanomaterials tend to exhibit high uptake in the reticuloendothelial system (RES) (liver, spleen, etc.) once injected into animals and are not rapidly excreted (6, 20). Whether or not and how these materials are cleared from the body is unknown in many cases, because of the difficulties in long term *in vivo* tracking and monitoring of the materials. Currently used radio labels (6, 20) or fluorescent labels for nanomaterials are useful for *in vivo* tracking over short periods of time (a few hours to a few days), but these labels may gradually dissociate from the materials or decay and lose activity over time. It is thus highly desirable to detect nanomaterials based on their intrinsic physical properties rather than relying on radiolabels or spectroscopic tags for indirect detection/measurement. The direct detection method may lead to a more accurate assessment of how nanomaterials behave *in vivo* in both short and long terms, i.e., during the blood circulation stage and during time periods lasting several months.

Here, we show that the intrinsic Raman scattering intensity of SWNTs (23, 24) does not decay over time while being relatively insensitive to the types of noncovalent coatings and solution environments of SWNTs. Unlike the resonance breathing model (RBM) in the SWNT Raman spectrum, the intensity of tangential graphene-like G band is relatively insensitive to the diameter and bundling of nanotubes (25, 26). We then use Raman spectroscopy to measure the postinjection blood concentration of SWNTs with different polyethylene-glycol (PEG) coatings in mice and thus glean nanotube blood circulation times. We also use Raman spectroscopy and Raman imaging to probe the biodistribution of SWNTs in various organs of mice *ex vivo* over a period of several months. We find that the surface chemistry, including the length and branching structure of PEG chains, is critical to the *in vivo* behaviors of SWNTs. Longer and more branched PEG on SWNTs afford longer blood circulation and lower RES uptake. Superior to linear PEG, branched PEG coating renders SWNTs a significantly prolonged blood circulation, which is desired for future targeted imaging or therapeutic applications. By monitoring the biodistribution of SWNTs in mice organs for months, a relatively slow, but persistent decrease in the SWNT Raman signal is observed, suggesting that the clearance of SWNTs is occurring in the mice. To study the excretion pathway, nanotubes with the highest possible dose is injected into mice with their excreta examined by Raman spectroscopy. Biliary excretion pathway is confirmed by the SWNT Raman signals in the intestine and feces. Although the SWNT concentration in urine is low over a high background,

Author contributions: Z.L., X.C., and H.D. designed research; Z.L., C.D., W.C., L.H., and X.C. performed research; C.D. contributed new reagents/analytic tools; Z.L. and C.D. analyzed data; and Z.L. and H.D. wrote the paper.

The authors declare no conflict of interest.

This article is a PNAS Direct Submission.

§To whom correspondence should be addressed. E-mail: hdai@stanford.edu.

This article contains supporting information online at www.pnas.org/cgi/content/full/0707654105/DC1.

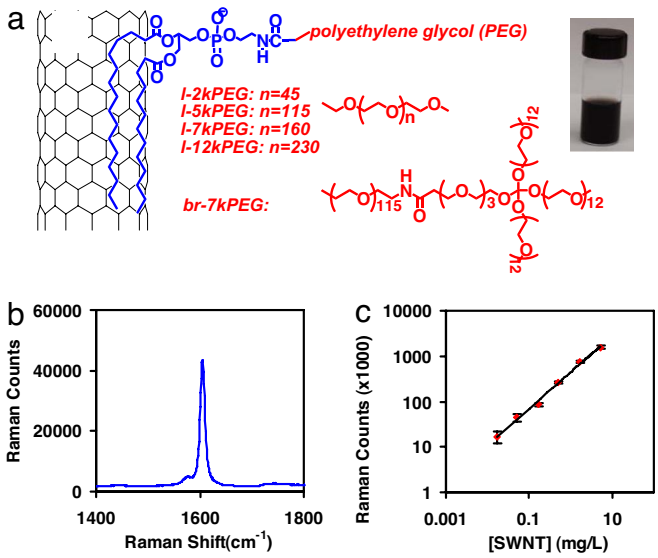

Fig. 1. Noncovalently functionalized SWNTs by various PEGylated phospholipids. (*a Left*) Scheme of functionalization by various phospholipid-PEGs with linear or branched PEG chains. (*Right*) A photo of the SWNT-*br*-7kPEG saline solution at the concentration (0.1 mg/ml; optical density was 4.6 at 808 nm for 1 cm path) used for injection. (*b*) A Raman spectrum of a solution of SWNT-*l*-2kPEG. The G band peak at 1,590 cm^{-1} was used for SWNT detection in this work. (*c*) Raman intensity vs. SWNT concentration calibration curve. Linear dependence was observed from 0.02 μg/ml to 4 μg/ml.

the existence of SWNT Raman signals in the kidney and bladder is evident, suggesting renal excretion for nanotubes as well. Further, necropsy, histology and blood chemistry studies reveal no obvious toxic effect for mice injected with SWNTs, providing further supports to the recent finding (M. L. Schipper, N. Nakayama-Ratchford, C.D., N. W. S. Kam, P. Chu, Z.L., X. Sun, L. C. Cork, H.D., and S. S. Gambhir, unpublished data). These results establish a foundation for further exploration of carbon nanotubes for biomedical applications and may have implications for other nanomaterials.

Results and Discussion

We used Hipco SWNTs noncovalently functionalized and solubilized (see *Materials and Methods*) by PEGylated phospholipids (Fig. 1*a*) that were stable without aggregation in various biological solutions including serum (15, 17, 20). Our previous study (20) also showed that the phospholipid-PEG coating was stable *in vivo* without rapid detachment. Centrifugation was used to remove big bundles and impurities, leaving short individual and small bundles of tubes in the solution. Atomic force microscopy (AFM) images revealed similar length distributions of different functionalized SWNTs [SWNT-*l*-2kPEG, 104 ± 49 nm; SWNT-*l*-5kPEG, 101 ± 51 nm; SWNT-*br*-7kPEG, 95 ± 46 nm; supporting information (SI) *Materials and Methods*, and SI Fig. 5]. Strong resonance Raman scattering is an intrinsic optical property of SWNTs with sharp peaks and low background in the spectra (Fig. 1*b*). In this work, the tangential graphite-like phonon mode (G band), the strongest peak in the SWNT Raman spectrum, was used to detect nanotubes in solution, blood, and tissue lysates. No obvious decay in the Raman signal was observed by measuring the Raman spectrum of a SWNT solution for up to 3 months (SI Fig. 6). Raman spectra of SWNT solutions with known concentrations from 0.02 to 4 μg/ml were taken, and the G band intensities (integrated peak areas) were plotted against SWNT concentrations [measured by their near infrared (NIR) absorptions] as the calibration curve (Fig. 1*c*). The linear dependence allowed for quantitative measurement of SWNT concentration in blood or tissue lysates of mice using Raman spectroscopy. Solutions of same concentration of SWNTs with different PEG coatings (SWNT-*l*-2kPEG and SWNT-*l*-5kPEG, SWNT-*br*-7kPEG) exhibited very similar Raman intensities in various environments including water, saline, lysis buffer, serum, and liver lysate. These results suggested that the Raman intensity of SWNTs was relatively insensitive to the coatings and solution environments involved in our experiments (SI Fig. 6).

We intravenously injected ≈200 μl of saline solutions of different PEG functionalized SWNTs at the same nanotube concentration (≈0.1 mg/ml) into mice and drew blood (≈5 μl) at different time points postinjection (p.i.) for Raman measurement (Fig. 2 *a–c*). The measured %ID/g (percentage of injected dose per gram) in blood vs. time p.i. gave blood circulation behavior of SWNTs with various PEGylations (Fig. 2 *d* and *e*). We observed that increasing the linear PEG chain length from 2 kDa (SWNT-*l*-2kPEG) to 5 kDa (SWNT-*l*-5kPEG) significantly extended the blood circulation of SWNTs from ≈1.2 h to ≈5 h (Fig. 2 *a*, *b*, *d*, and *e*). Note that we defined the blood circulation time as the time span over which the blood SWNT level reduced to 5%ID/g. This result was consistent with our previous measurements made with radio-labeled SWNTs (20). However, further increase of linear PEG length to 7 kDa (SWNT-*l*-7kPEG) and even 12 kDa (SWNT-*l*-12kPEG) showed only minor effect on the blood circulation time (Fig. 2 *d* and *e*). However, SWNT-*br*-7kPEG, i.e., SWNTs functionalized with three branched PEG chains (Fig. 1*a*), exhibited a remarkable increase in circulation to ≈15 h (Fig. 2 *c*, *d*, and *e*, with SWNTs detected in the blood nearly 1 day p.i.). This finding is important and suggests that branched PEG structures on SWNTs is highly desired in affording optimal biological inertness of SWNTs that resist opsonization or nonspecific binding of proteins *in vivo*, avoiding rapid RES uptake and thus prolonging circulation in blood. We attribute this improvement to the branched PEG structure giving better coverage and higher density of hydrophilic PEG groups on SWNTs, thus making nanotubes more inert and resistant to nonspecific binding and uptake.

To investigate the biodistribution of nanotubes in the main organs 1 day p.i. of SWNTs, we killed mice injected with SWNT-*l*-2kPEG, SWNT-*l*-5kPEG, and SWNT-*br*-7kPEG, respectively. The organs and tissues were homogenized and solubilized in lysis buffers, for measuring SWNT levels in these organs and tissues by Raman spectroscopy (Fig. 3*a* and SI Fig. 7). We observed dominant SWNT uptake in the liver and spleen of the RES over other organs and tissues. Clearly reduced levels of liver and spleen uptake were seen for SWNT-*l*-5kPEG and SWNT-*br*-7kPEG compared with SWNT-*l*-2kPEG (Fig. 3*a*), suggesting higher degree of surface PEGlyation of SWNTs affording lower RES uptake. Under the injected dose of 200 μl of SWNT at ≈0.1 mg/ml concentration and detection conditions, no obvious SWNT signals were detected in other main organs except for minor kidney signal. Note that the detection limit of SWNTs was ≈0.04 μg/ml in blood and ≈0.2 μg/ml in other tissues, corresponding to ≈0.2%ID/g and ≈1%ID/g of the normal injected dose respectively. Therefore, under the injected ≈200 μl of ≈0.1 mg/ml nanotubes, the lack of appreciable SWNT Raman signals in organs other than liver, kidney, and spleen (Fig. 3*a*) does not mean absolutely no SWNT uptake in those organs. It suggests only that the level of uptake is lower than a certain limit (1–2%ID/g). The total amount of SWNTs in these organs could still be substantial owing to the large mass/weight of the tissues combined.

Indeed, by injecting a highly concentrated SWNT-*l*-5kPEG solution (200 μl of ≈0.5 mg/ml SWNTs in a form of concentrated viscous liquid) into mice, we observed at 1 day p.i. that, besides dominant liver and spleen uptake, SWNT Raman signals became apparent in the bone (leg bone), kidney, intestine, stomach, and lung of mice with ≈1%ID/g in the first three organs (Fig. 4*a*).

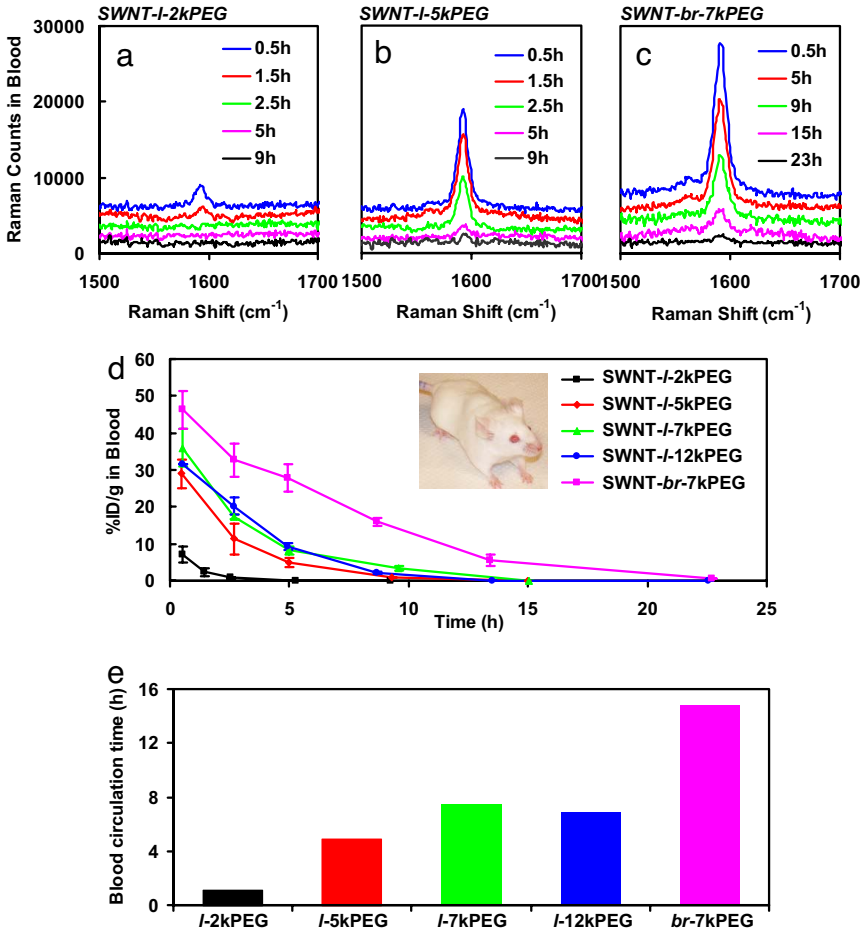

Fig. 2. Blood circulation behavior of SWNTs probed by Raman spectroscopy. (*a–c*) Raman spectra of blood samples drawn from BALB/c mice at various time points after injection with SWNT-*l*-2kPEG (*a*) SWNT-*l*-5kPEG (*b*), and SWNT-*br*-7kPEG (*c*) solutions, respectively. Note that spectrum baselines were subtracted in *a–c*. (*d*) Blood circulation data probed by the Raman method for SWNT-*l*-2kPEG, SWNT-*l*-5kPEG, SWNT-*l*-7kPEG, SWNT-*l*-12kPEG, and SWNT-*br*-7kPEG. Injected into BALB/c mice (*Inset*). The SWNT levels in blood were determined as percentage of injected SWNT amount per gram of blood (%ID/g in blood). SWNT-*l*-5kPEG, SWNT-*l*-7kPEG, and SWNT-*l*-12kPEG showed similar blood circulation time, significantly longer than that of SWNT-*l*-2kPEG. The longest blood circulation was observed for SWNT-*br*-7kPEG. The error bars are based on four mice in each group. (*e*) Blood circulation time of SWNTs with different PEGylations. The blood circulation time was defined as the time duration through which the blood SWNT level reduced to 5%ID/g.

Because bone marrow is part of the RES, uptake of SWNTs in the bone is understandable and consistent with the previous biodistribution study for other nanomaterials (27). The existence of SWNTs in the kidney and intestine of mice is interesting, suggesting possible urinary and biliary excretion routes for SWNTs, as discussed in the following paragraphs.

To glean the long term fate of SWNTs *in vivo*, injected mice were killed at 1, 2, and 3 months p.i. for biodistribution measurements with three to four animals per group at each time point. We found that the concentration of SWNTs remained very low in most of the organs except for the liver and spleen. In these two organs, we did observe SWNT levels steadily decreasing over a 3-month period, with the concentration of retained SWNTs following the trend of SWNT-*l*-2kPEG > SWNT-*l*-5kPEG > SWNT-*br*-7kPEG at later time points (Fig. 3 *b* and *c*). In the case of SWNT-*l*-2kPEG, appreciable amounts of SWNTs remained in the liver and spleen, with a concentration of ≈7%ID/g at even 3 months p.i. In contrast, very low levels (≈2%ID/g) of SWNT-*l*-5kPEG were retained in the RES of mice at 3 months p.i. (Fig. 3 *b* and *c*). The least retention of nanotubes in the RES was observed for SWNT-*br*-7kPEG, with <2%ID/g retention at 2 months p.i. These results suggest that, in addition to the advantages of longer blood circulation and lower initial RES uptake, higher degree of PEGylation of SWNTs affords more rapid clearance of SWNTs from mice organs, with branched PEG functionalization giving the most desirable *in vivo* behavior of SWNTs. We also carried out Raman spectroscopic mapping and imaging of SWNTs in the liver slices of mice at the 3-month time point. Many "hot spots" (locations over the liver slice showing high SWNT Raman signals) were observed in the SWNT-*l*-2kPEG treated sample and few in the SWNT-*l*-5kPEG-treated sample (Fig. 3*d*). This observation was consistent with much lower level of SWNT retention in the liver in the latter case.

Because no significant SWNT signals were detected in the main organs of mice other than in the RES over the several-month period, we suggest that the clearance of SWNTs from the RES was due to the excretion of SWNTs out of the body, rather than nanotubes migrating to other organs of mice. The excretion occurred faster for SWNTs with higher degree of PEGylation, hydrophilicity, and biological inertness. To find out the detailed excretion pathway, we collected the urine and feces of mice at different time points after injection of high doses of SWNTs and carried out Raman measurement. We observed appreciable SWNT Raman signal in the dry feces sample of mice after subtracting a high background (Fig. 4*c*). The obvious presence of nanotubes in the feces and intestine (Fig. 4*b*) clearly reveals SWNT excretion via the biliary pathway in the feces. Although no significant SWNT Raman signal was observed in the urine

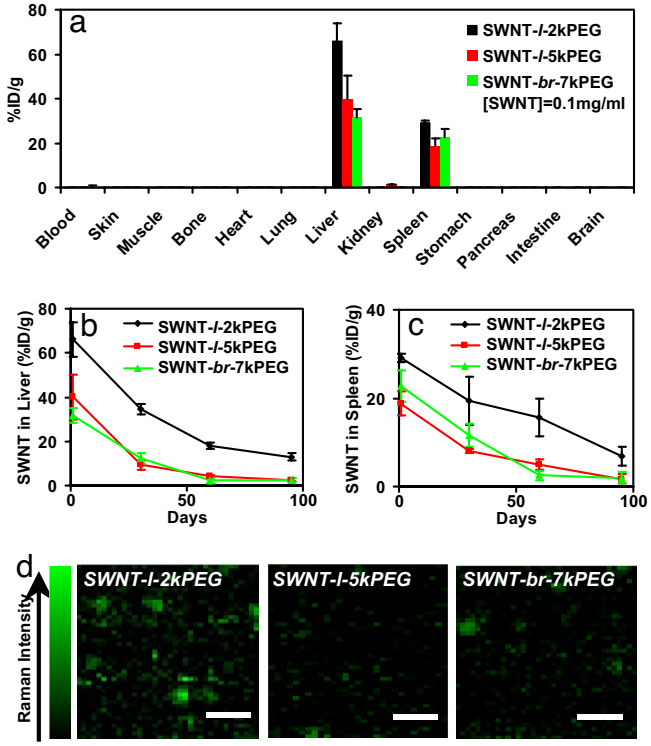

Fig. 3. SWNTs in mice tissues probed by *ex vivo* Raman spectroscopy after injection into mice. (*a*) Biodistribution of SWNT-*l*-2kPEG, SWNT-*l*-5kPEG, and SWNT-*br*-7kPEG, respectively, at 1 day p.i. measured by Raman spectroscopy. The SWNT concentrations in most organs are below detection limit. (*b* and *c*) Evolution of the concentrations of SWNTs retained in the liver and spleen of mice over a period of 3 months. Compared with SWNT-*l*-2kPEG, much lower concentrations of retained SWNTs in the liver and spleen were observed for SWNT-*l*-5kPEG and SWNT-*br*-7kPEG. (*d*) Raman mapping images of liver slices from mice treated with SWNT-*l*-2kPEG (*Left*), SWNT-*l*-5kPEG (*Center*), and SWNT-*br*-7kEG (*Right*)at 3 months p.i. More SWNT signals were observed in the SWNT-*l*-2kPEG-treated mouse sample than the other two samples under the same Raman imaging conditions (laser power, beam size, etc.). The error bars in *a*–*c* were based on three to four mice per group. Note that the injected SWNT solutions had a concentration of 0.1 mg/ml (optical density was 4.6 at 808 nm for 1 cm path).

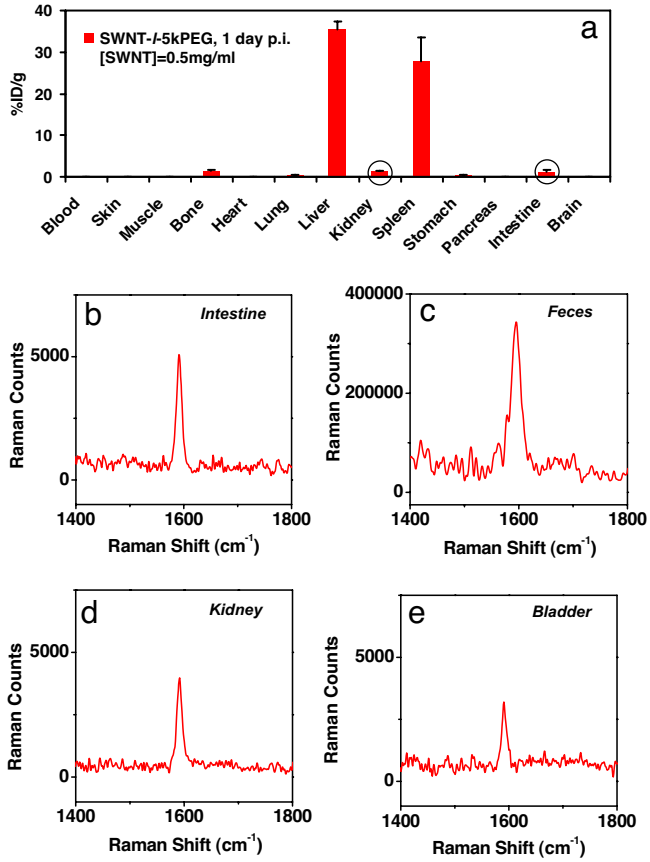

Fig. 4. Biodistribution measured under ultra-high dose SWNT (0.5 mg/ml) injection. (*a*) Biodistribution of SWNT-*l*-5kPEG in various organs of mice received 200 μl of 0.5 mg/ml SWNT-*l*-5kPEG at 24 h p.i. After increasing of the injected dose, SWNTs became detectable by Raman in several organs including bone, lung, kidney, stomach, and intestine, with slightly over 1%ID/g in bone, kidney and intestine. Error bars were based on three mice. (*b* and *c*) Raman spectra of intestine lysate at 24 h p.i. (*b*) and dry feces sample collected 8 h p.i. (*c*). Because of high background in the feces sample, the spectrum was taken by 600 s long time collection (5 s for all of the other samples). An appreciable amount of nanotubes was noticed in the intestine and feces, providing clear evidence for the biliary excretion pathway of intravenously injected SWNTs. (*d* and *e*) Raman spectra of kidney (*d*) and bladder (*e*) lysates from mice at 24 h p.i. The existence of SWNTs in the kidney and bladder indicate that a small portion of nanotubes is excreted via the kidney-urine pathway. Note that background has been subtracted in the spectra *b*–*e*.

samples because of high background and dilution by large urine volume, we did observe clear SWNT signals in the kidney and bladder of mice at 24 h p.i. (Fig. 4 *d* and *c*). Further, for mice injected with SWNTs at 3 days p.i., SWNT signals in the kidney were much lower and almost nonexistent in the bladder (data not shown). This finding suggests that SWNTs were also excreted through the renal pathway. Considering the average lengths of SWNTs (mean $\approx$100 nm, SI Fig. 5) exceeding the renal excretion threshold (28) and the fact that the majority of nanotubes accumulates in the liver, we suggest that urinary excretion occurs for a small percentage of nanotubes with very short length (<50 nm in length, diameter 1–2 nm) in our sample at early time points after injection. Because of the existence of nanotubes in feces, the nonbiodegradable nature of sp^2 carbon SWNT structure and the fact that foreign nondegradable substances (including various nanoparticles) in the liver are known to be excreted through the biliary pathway from the liver to the bile duct, intestine, and feces (29–35), we propose that excretion of our SWNTs from mice occurs over time mainly via the biliary pathway and ends up in feces.

Notably, our results here including the dominant RES uptake of SWNTs and the relatively slow excretion are consistent with several previous reports by us (20) and other groups (21, 22) who used detection methods based on strongly anchored serum-stable radiolabels on SWNTs or the intrinsic Raman, photoluminescence or isotope properties of the nanotube themselves. The slow excretion contradicts with the report by Singh *et al* (36), who suggested fast urinal excretion of carbon nanotubes based on radiolabel signals, which could be due to detachment of radiolabels from nanotubes or free unconjugated excess radiolabels in the injected samples. Such problems are avoided in direct detection methods using the intrinsic physical or chemical properties of nanotubes.

Neither mortality nor significant loss of body weight was observed with any of the mice (>30) injected with 0.1 mg/ml SWNTs during the 3-month period of the study. To investigate any potential toxic effect of SWNTs, necropsy, histology and blood chemistry examinations were performed on our SWNT treated mice at 3 months p.i. No obvious toxicity of nanotubes was noticed in this small-scale toxicity study (SI Fig. 8 and SI Table 1). This observation is consistent with a recent pilot toxicity study carried out with four to five mice per group injected with similarly functionalized nanotubes (M. L. Schipper,

N. Nakayama-Ratchford, C.D., N. W. S. Kam, P. Chu, Z.L., X. Sun, L. C. Cork, H.D., and S. S. Gambhir, unpublished data). These two independent studies combined provide a strong indication of the lack of toxicity of well functionalized SWNTs in mice before clearance from the body. In contrast to a previous study of nonfunctionalized pristine carbon nanotubes causing fiber toxicity to mice (37), our well functionalized SWNTs are highly biocompatibility for *in vivo* applications. The functionalization chemistry of nanotubes is critical to the *in vivo* behaviors of nanotubes, including blood circulation, retention, excretion, and toxicity.

Conclusion

We have shown in the current work that the Raman spectroscopy can be used to detect carbon nanotubes in animals to glean the blood circulation behavior and biodistribution in main organs, especially in the RES. The robust Raman scattering property of SWNTs allows us to track them for a long period with high fidelity, without the concern of labels falling off or decay over time. It is found that the surface chemistry of nanotubes is critical to their *in vivo* behavior, a conclusion that will likely apply to most nanomaterials, if not all. This result is expected because pristine carbon nanotubes have very hydrophobic surfaces and are highly nonspecific in binding to biological species (38, 39). Recently, it has been shown that intravenously injected pristine SWNTs are highly rich in the lung as well as RES and remain in mice indefinitely (22). This hydrophobicity has to be blocked by proper chemical functionalization such as the PEG coatings described here, which enables biologically inert SWNTs with long blood circulation, low RES uptake, and relatively fast clearance from organs and excretion from the body. The degree of PEGylation of SWNTs is important to the *in vivo* behaviors of nanotubes. Longer PEG chains, especially those with branched structures, are excellent in affording SWNTs with the most desirable characteristics for *in vivo* applications. This result should also be applicable to functionalization of various other nanomaterials (nanocrystals, particles, etc.) for *in vivo* research. SWNTs detected in the feces of mice clearly reveal the biliary excretion pathway. A small percentage of nanotubes seems to be excreted via the renal pathway. Last, no obvious toxic effect is found in the necropsy, histology, and blood chemistry studies, which warrants the safety of properly functionalized carbon nanotubes for future *in vivo* biomedical applications.

Materials and Methods

Various PEGylated Phospholipids (PL-PEGs) Used for Noncovalent Functionalization of Nanotubes. Several PL-PEGs with linear PEG structure and one PL-PEG with branched PEG structure were used in this study (Fig. 1*a*) including commercially available DSPE-PEG(2000)Amine (denoted as ''L-*l*-2kPEG''where *l* stands for linear, Avanti) and SUNBRIGHT DSPE-050PA (PL-*l*-5kPEG, NOF cooperation). PL-*l*-7kPEG was synthesized by mixing 1 eq of DSPE-050PA with 2 eq of NHS-mPEG2000 (Nektar) in methylene chloride overnight followed by addition of 2 eq of N,N′-dicyclohexylcarbodiimide (DCC, Aldrich). DCC was used to reactivate any potentially hydrolyzed NHS group on PEG during storage. The solvent was evaporated after another 24 h reaction. Water was added, and the insoluble solid (unreacted DCC) was removed by vacuum filtration. The final product was a clear water solution and was stored at −20°C for future usage. PL-*l*-12kPEG and PL-*br*-7kPEG (where *br* stands for ''branched'') were synthesized by similar methods except for the starting materials. One eq of DSPE-PEG(2000)Amine and 2 eq of NHS-mPEG10000 (Nektar) were used to synthesize PL-*l*-12kPEG whereas 1 eq of DSPE-050PA and 1.5 eq of (Methyl-PEO_{12})$_3$-PEO_4-NHS Ester (Pierce) were used to make PL-*br*-7kPEG. The final products were characterized and confirmed (data not shown) by MALDI (matrix-assisted laser desorption/ionization) mass spectrometry in Stanford PAN facility, showing no existence of starting PL-*l*-5kPEG or PL-*l*-2kPEG materials. No further purification was performed because the excess hydrophilic NHS-PEG molecules were confirmed to exhibit no binding affinity to the hydrophobic nanotube surface. The excess NHS-PEGs were removed during the nanotube filtration step.

Fuctionalization and Characterization of PEGylated SWNTs. Raw Hipco SWNTs (0.2 mg/ml) were sonicated in a 0.2-mM solution of PL-PEG for 1 h followed by centrifugation at 24,000 × *g* for 6 h, yielding a suspension of SWNTs with noncovalent PL-PEG coating in the supernatant (15, 20, 40). Excess surfactant and unreacted PEG molecules in the case of synthesized PL-PEG were removed by filtration through a 100-kDa MWCO filter (Millipore), typically 1 day before *in vivo* experiments. The filtration efficiency was confirmed by fluorescent labeled PEG, showing completed removal of PEG molecules after 6 times filtration and washing (data not shown). Right before injection, the solution was centrifuged again at 24,000 × *g* for 6 h to remove any potential aggregates. UV-VIS-NIR absorption spectrum of the SWNT solution was acquired by a Cary 6000i UV-visible-NIR spectrometer. Atomic force microscopy (AFM) images were taken by depositing SWNTs from solution onto SiO_2 substrates. The length of SWNTs was measured to be ≈100 nm averaged over 100 tubes imaged by AFM. The concentration of a SWNT solution was determined by Raman spectroscopy and by optical absorbance at 808 nm with a weight-concentration based extinction coefficient of 46 $L \cdot g^{-1} \cdot cm^{-1}$ or a molar extinction coefficient of 3.9×10^6 $M^{-1} \cdot cm^{-1}$ for typical ≈100-nm-long tubes (11).

Raman Measurement of SWNT Solutions for Calibration Curve of SWNT Raman Intensity vs. Concentration. SWNT solutions of various concentrations in capillary glass tubes (Fisher) were measured by using a Renishaw microRaman instrument (laser excitation wavelength = 785 nm). A glass capillary tube filled with a SWNT solution was placed under the objective (×20) of the Raman microscope. As low as 2 μl of solution sample was required for each measurement. After focusing at the center of the capillary, we recorded the Raman spectrum of the solution (100 mW power with laser spot size of ≈25 μm^2, 10-s collection time). At least four spectra were taken for each sample for averaging. For a given concentration of SWNT solution, the Raman intensity was obtained by integrating the SWNT G-band peak area from 1,570 cm^{-1} to 1,620 cm^{-1} and averaged over several spectra. Note that SWNTs with the same concentration in water, buffer, serum, and tissue lysate were found to exhibit similar Raman intensities (see SI Fig. 6).

SWNT i.v. Injection and Raman Spectroscopy Method for Measuring Blood Circulation and Biodistribution in Mice. Six-week-old BALB/c mice were used in our study. Two hundred microliters of ≈0.1 mg/ml SWNT (optical density was 4.6 at 808 nm for 1 cm path) saline solution was intravenously (i.v.) injected into the tail vein of each mouse. Before injection of the SWNT solution, a Raman spectrum was recorded and used to calculate the SWNT concentration based on the calibration curve described above. At various time points postinjection (p.i.), ≈5 μl of blood was collected from the tail vein (using a different vein from the injected one) and dissolved in 5 μl of lysis buffer (1% SDS, 1% Triton X-100, 40 mM Tris acetate, 10 mM EDTA, 10 mM DTT) for detecting SWNTs in the blood by Raman measurement. The Raman G band peak areas were measured to calculate the SWNT concentrations in the blood. The percent injected dose per gram (%ID/g) of blood was calculated by the following equation:

$$\%\mathrm{ID/g} = \frac{[\mathrm{SWNT}]_{\mathrm{blood\ lysate}} \times \mathrm{V}_{\mathrm{blood\ lysate}}}{[\mathrm{SWNT}]_{\mathrm{injected}} \times \mathrm{V}_{\mathrm{injected\ SWNT}} \times \mathrm{blood\ weight}} \times 100\%.$$

For biodistribution study performed at ultra-high SWNT dose, 4 ml of SWNT-*l*-5kPEG solution with normal concentration (0.1 mg/ml) was concentrated down to 0.8 ml of (0.5 mg/ml) by filtration through a 100-kDa filter. The solution was a black liquid with an optical density >20 at 808 nm (1-cm path length).

For biodistribution study, mice were killed at 1, 30, 60, and 90 days p.i., and the organs/tissues were collected, weighed, and solubilized in the lysis buffer using a homogenizer (strong stirring and sonication, 1 min for each sample). After heating at 70°C for ≈2 h, clear homogenate tissue solutions were obtained for Raman measurement. A control experiment was done to confirm that this treatment did not affect the Raman intensity of an SWNT solution (data not shown). The biodistribution of SWNTs in various organs of mice was then calculated and plotted in unit of %ID/g based on the following equation,

$$\%\mathrm{ID/g} = \frac{[\mathrm{SWNT}]_{\mathrm{tissue\ lysate}} \times \mathrm{V}_{\mathrm{tissue\ lysate}}}{[\mathrm{SWNT}]_{\mathrm{injected}} \times \mathrm{V}_{\mathrm{injected\ SWNT}} \times \mathrm{tissue\ weight}} \times 100\%.$$

We used three to four mice per group at each time point p.i. to obtain the average value and standard deviation for both blood circulation and biodistribution measurements.

We also used a microRaman technique (15) to carry out Raman imaging of SWNTs in liver slices. To obtain the Raman mapping image of liver slices (for mice killed at 90 days p.i.), 5-μm-thick paraffin-embedded liver slices were mounted on SiO_2 substrate and mapped under a Renishaw microRaman microscope with a line-scan model (100 mW laser power, 40 μm $\times$ 2 μm laser spot size, 20 pixels each line, 2-s collection time, $\times$20 objective). The SWNT G-band Raman intensity was plotted vs. *x* and *y* positions across the liver slice to obtain a Raman image.

ACKNOWLEDGMENTS. This work was supported in part by the National Institutes of Health-National Cancer Institute (NIH-NCI) Center for Cancer Nanotechnology Excellence Focused on Therapy Response (CCNE-TR) at Stanford, a Stanford BioX grant, a Stanford Graduate Fellowship, and a Benedict Cassen Postdoctoral Fellowship from the Education and Research Foundation of the Society of Nuclear Medicine.

1. Whitesides GM (2003) The ''right'' size in nanobiotechnology. *Nat Biotech* 21:1161–1165.
2. Service RF (2005) Nanotechnology takes aim at cancer. *Science* 310:1132–1134.
3. Sinha R, Kim GJ, Nie SM, Shin DM (2006) Nanotechnology in cancer therapeutics: Bioconjugated nanoparticles for drug delivery. *Mol Cancer Ther* 5:1909–1917.
4. Gao XH, Cui YY, Levenson RM, Chung LWK, Nie SM (2004) *In vivo* cancer targeting and imaging with semiconductor quantum dots. *Nat Biotech* 22:969–976.
5. Farokhzad OC, *et al*. (2006) Targeted nanoparticle-aptamer bioconjugates for cancer chemotherapy *in vivo*. *Proc Natl Acad Sci USA* 103:6315–6320.
6. Lewin M, *et al*. (2000) Tat peptide-derivatized magnetic nanoparticles allow *in vivo* tracking and recovery of progenitor cells. *Nat Biotech* 18:410–414.
7. Maier-Hauff K, *et al*. (2007) Intracranial thermotherapy using magnetic nanoparticles combined with external beam radiotherapy: Results of a feasibility study on patients with glioblastoma multiforme. *J Neurooncol* 81:53–60.
8. Chen CC, *et al* (2006) DNA-gold nanorod conjugates for remote control of localized gene expression by near infrared irradiation. *J Am Chem Soc* 128:3709–3715.
9. Zheng GF, Patolsky F, Cui Y, Wang WU, Lieber CM (2005) Multiplexed electrical detection of cancer markers with nanowire sensor arrays. *Nat Biotech* 23:1294–1301.
10. Bianco A, Kostarelos K, Partidos CD, Prato M (2005) Biomedical applications of functionalised carbon nanotubes. *Chem Commun* 571–577.
11. Kam NWS, O'Connell M, Wisdom JA, Dai HJ (2005) Carbon nanotubes as multifunctional biological transporters and near-infrared agents for selective cancer cell destruction. *Proc Natl Acad Sci USA* 102:11600–11605.
12. Chen X, Kis A, Zettl A, Bertozzi CR (2007) A cell nanoinjector based on carbon nanotubes. *Proc Natl Acad Sci USA* 104:8218–8222.
13. Dai H (2002) Carbon nanotubes: Synthesis, integration, and properties. *Acc Chem Res* 35:1035–1044.
14. Dresselhaus M, Dai H, eds (2004) MRS 2004 Carbon Nanotube Special Issue (Materials Research Society, Warrendale, PA), Vol 29.
15. Liu Z, Winters M, Holodniy M, Dai HJ (2007) siRNA delivery into human T cells and primary cells with carbon-nanotube transporters. *Angew Chem Inter Ed* 46:2023–2027.
16. Liu Y *et al* (2005) Polyethylenimine-grafted multiwalled carbon nanotubes for secure noncovalent immobilization and efficient delivery of DNA. *Angew Chem Inter Ed* 44:4782–4785.
17. Kam NWS, Liu Z, Dai HJ (2005) Functionalization of carbon nanotubes via cleavable disulfide bonds for efficient intracellular delivery of siRNA and potent gene silencing. *J Am Chem Soc* 36:12492–12493.
18. Feazell RP, Nakayama-Ratchford N, Dai H, Lippard SJ (2007) Soluble single-walled carbon nanotubes as longboat delivery systems for platinum(IV) anticancer drug design. *J Am Chem Soc* 129:8438–8439.
19. Liu Z, Sun X, Nakayama N, Dai H (2007) Supramolecular chemistry on water-soluble carbon nanotubes for drug loading and delivery. *ACS Nano* 1:50–56.
20. Liu Z, *et al*. (2007) *In vivo* biodistribution and highly efficient tumour targeting of carbon nanotubes in mice. *Nat Nanotech* 2:47–52.
21. Cherukuri P, *et al*. (2006) Mammalian pharmacokinetics of carbon nanotubes using intrinsic near-infrared fluorescence. *Proc Natl Acad Sci USA* 103:18882–18886.
22. Yang S-t, *et al*. (2007) Biodistribution of pristine single-walled carbon nanotubes *in vivo*. *J Phys Chem C* 11:17761–17764.
23. Richter E, Subbaswamy KR (1997) Theory of size-dependent resonance Raman scattering from carbon nanotubes. *Phys Rev Lett* 79:2738–2741.
24. Jorio A, *et al*. (2001) Structural (n,m) determination of isolated single-wall carbon nanotubes by resonant Raman scattering. *Phys Rev Lett* 86:1118–1121.
25. Peters MJ, McNeil LE, Lu JP, Kahn D (2000) Structural phase transition in carbon nanotube bundles under pressure. *Phys Rev B* 61:5939–5944.
26. Rao AM, *et al*. (1997) Diameter-selective Raman scattering from vibrational modes in carbon nanotubes. *Science* 275:187–191.
27. Cai WB, *et al*. (2006) Peptide-labeled near-infrared quantum dots for imaging tumor vasculature in living subjects. *Nano Lett* 6:669–676.
28. Fang J, Sawa T, Akaike T, Maeda H (2002) Tumor-targeted delivery of polyethylene glycol-conjugated D-amino acid oxidase for antitumor therapy via enzymatic generation of hydrogen peroxide. *Cancer Res* 62:3138–3143.
29. Hori Y, Ohyanagi H (1994) Biliary-excretion of lipopolysaccharide is microtubule-dependent in isolated-perfused rat-liver. *J Gastroenter* 29:800–801.
30. Liu Y, *et al*. (2000) Pharmacokinetics and hepatic disposition of bis[1-(ethoxycarbonyl)-propyl]5-acetylamino-2,4,6-triiodoisophthalate in rats and isolated perfused rat livers. *Drug Metab Dispos* 28:731–736.
31. Nefzger M, Kreuter J, Voges R, Liehl E, Czok R (1984) Distribution and elimination of poly(methyl methacrylate nanoparticles after peroral administration to rats. *J Pharm Sci* 73:1309–1311.
32. Jani PU, *et al*. (1996) Biliary excretion of polystyrene microspheres with covalently linked FITC fluorescence after oral and parenteral administration to male Wistar rats. *J Drug Target* 4:87–91.
33. Ogawara K, *et al*. (1999) Uptake by hepatocytes and biliary excretion of intravenously administered polystyrene microspheres in rats. *J Drug Target* 7:213–217.
34. Furumoto K, *et al*. (2001) Biliary excretion of polystyrene microspheres depends on the type of receptor-mediated uptake in rat liver. *Biochim Biophys Acta* 1526:221–226.
35. Dupas B, *et al*. (1999) Electron microscopy study of intrahepatic ultrasmall superparamagnetic iron oxide kinetics in the rat: Relation with magnetic resonance imaging. *Biol Cell* 91:195–208.
36. Singh R, *et al*. (2006) Tissue biodistribution and blood clearance rates of intravenously administered carbon nanotube radiotracers. *Proc Natl Acad Sci USA* 103:3357–3362.
37. Donaldson K, *et al*. (2006) Carbon nanotubes: A review of their properties in relation to pulmonary toxicology and workplace safety. *Toxicol Sci* 92:5–22.
38. Chen RJ, *et al*. (2003) Noncovalent functionalization of carbon nanotubes for highly specific electronic biosensors. *Proc Natl Acad Sci USA* 100:4984–4989.
39. Shim M, Kam N, Chen R, Li Y, Dai H (2002) Functionalization of carbon nanotubes for biocompatibility and biomolecular recognition. *Nano Lett* 2:285–288.
40. Kam NWS, Liu Z, Dai HJ (2005) Functionalization of carbon nanotubes via cleavable disulfide bonds for efficient intracellular delivery of siRNA and potent gene silencing. *J Am Chem Soc* 127:12492–12493.